Supplementary Materials for

Reconfigurable ferromagnetic liquid droplets

Xubo Liu, Noah Kent, Alejandro Ceballos, Robert Streubel, Yufeng Jiang, Yu Chai, Paul Y. Kim, Joe Forth, Frances Hellman, Shaowei Shi, Dong Wang, Brett A. Helms, Paul D. Ashby, Peter Fischer, Thomas P. Russell*

*Corresponding author. Email: tom.p.russell@gmail.com

Published 19 July 2019, *Science* **365**, 264 (2019)
DOI: 10.1126/science.aaw8719

This PDF file includes:

Materials and Methods
Figs. S1 to S5
Table S1
Captions for Movies S1 to S10
References

Other Supplementary Material for this manuscript includes the following:
(available at science.sciencemag.org/content/365/6450/264/suppl/DC1)

Movies S1 to S10

Materials and Methods

Chemicals

The following chemicals were used as received from Sigma-Aldrich: Carboxyl-modified iron oxide nanoparticles, (Fe_3O_4-CO_2H NPs, 30 nm). The iron oxide core with 22 nm diameter was coated with a 4 nm thin layer of polymer ligands with carboxyl-end-functionalized, forming a periphery of charged units that stabilizes the NPs dispersion in water; Polyethylene glycol coated iron oxide nanoparticles, (Fe_3O_4-PEG NPs, 30 nm); Amine-modified polyhedral oligomeric silsesquioxane (POSS-NH_2, M_w = 917 g mol^{-1}), Toluene (> 99.8%); Carbon tetrachloride (> 99.9%); Hydrochloric acid (37%); Nile Red (> 98%); Fluorescein sodium salt (acid yellow 73, M_w = 376 g mol^{-1}); Rhodamine B (> 95%); Sodium carboxymethyl cellulose (CMC-CO_2Na, M_w = ~90 Kg mol^{-1}).

Magnetism characterization

A vibrating sample magnetometer (Lakeshore) was used to measure the M-H hysteresis loop of the liquid droplets at room temperature (shown in Fig. S2). For the jamming state of single droplets, the droplet containing a dispersion of MNPs (1, 5 and 9 μL respectively, pH 4.5, [Fe_3O_4-CO_2H MNPs] = 0.5 g L^{-1}) was immersed in ~50 μL of pure toluene ([POSS-NH_2] = 1.0 g L^{-1}) and sealed in a liquid sample holder (730935 Kel-F liquid disposable cup, Lakeshore) for measurements within 2 hr. For the jamming state of emulsified droplets with volume of 5 and 9 μL, the droplet containing MNPs (pH 4.5, [Fe_3O_4-CO_2H MNPs] = 0.5 g L^{-1}) was sealed in the holder and then emulsified by ultrasonication for 10 s. For the unjamming state, pH of the droplets was tuned to 4.5, 7.0, and 9.5 at MNPs concentration of 0.5 g L^{-1}, and pH 4.5 at MNPs concentration of 0.05 g L^{-1}, all of those droplets immersed in the toluene containing 0.01 g L^{-1} of POSS-NH_2, by which the droplet surface cannot reach fully coverage state during the vibrating sample magnetometer measurements.

Measurement of interfacial tensions and surface coverages

An example of the interfacial tension between water and toluene measured with a tensiometer (KRÜSS GmbH, DSA30) is shown in Fig. S1A, B. The surface coverage $C_s = S_{wrinkling}/S_{free}$ of the MNPs-surfactants at the water/toluene interface was estimated using a pendant drop from the initial volume (surface area, S_{free}) and from the volume of the droplet (surface area, $S_{wrinkling}$) at which the assembly of the MNP-surfactants jammed and began to wrinkle. The droplet is assumed to be rotationally symmetric. The results are shown in Fig. S1C. The higher the surface coverage, the less the droplet volume must be reduced before wrinkling is observed.

AFM imaging

An atomic force microscope (AFM, Bruker, Icon) was used to measure the diameter and morphology of MNPs assembled at the water/toluene interface. The assembled film at the water/toluene interface when jamming occurred was retrieved from the liquid interface using a clean silicon wafer and dried at ambient conditions. The AFM image shown in Fig. S4B indicates that the diameter of MNPs at the interface is ~30 nm.

TEM imaging

We transferred a monolayer of jammed NPs to a silicon nitride wafer for TEM imaging. From the TEM image, the particles are ~30 nm. Some particles are quite anisotropic in shape. Depending on the angle between the lattice of the iron oxide atoms and the electron beam, the contrast of the

particles will vary. The iron oxide core is also wrapped by a 3~4 nm layer of carboxyl end-functionalized polyetheleneglycol (PEG). The in-surface shape anisotropy leads to disordered packing structure. The nearest-neighbor numbers typically varying from 5 to 8. Images were taken at room temperature using full-field TEM mode with an acceleration voltage of 300 kV (TEAM-1).

Fabrication of liquid cylinders

Using all-liquid 3D printing in a microfluidic device, we continuously printed all-liquid cylinders of the FLD. Upon printing, a slight decrease in the interfacial area jams the MNP-surfactants that form and assemble at the interface. In particular, 2 mm long liquid cylinders with a diameter of 1 mm were printed through a 1 mm diameter PTFE tube, as shown in Fig. S3, by setting a flow rate of the continuous oil phase containing ligands, $Q_O = 30$ μL min^{-1}, and that of the aqueous dispersion of Fe_3O_4-CO_2H MNPs, $Q_W = 90$ μL min^{-1}, respectively. The shape of FLD droplet changes from spherical to cylindrical when $Q_W/Q_O > 1$. If Q_W/Q_O is large enough, a continuous filament of the aqueous phase can be printed in the oil phase. Within the capillary, the interface of droplets from spherical to cylindrical shape undergo extensive plastic deformation, with the droplet's shape governed by both surface wetting properties of the droplet against the glass or PTFE pipette and the complex mechanical properties of the disordered MNPS assembly *(19, 20)*.

Fabrication of electromagnetic solenoid

An aluminum wire with ~0.2 mm diameter was wound into a solenoid to generate current-induced magnetic fields that interact with the FLDs. The setup provided a magnetic field of up to 1~2 kA m^{-1} at the center of the solenoid using a current of $I = 2$ A and $N = 15$ windings, each separated by $L = 1$~2 mm. The measured value is in good agreement with the analytical value of $H = I/L = 1$~2 kA m^{-1}.

Fabrication of density gradient oil phase

The solubility of toluene and CCl_4 in water are 0.051% *w/w* and 0.08% *w/w*, and the dynamic viscosity of toluene and CCl_4 at 20 ˚C are 0.59 cp and 0.97 cp, respectively. They are immiscible with water. Toluene (0.865 g cm^{-3}) is able to segregate and form a thin layer on top of CCl_4 phase (1.595 g cm^{-3}) without fierce shaking, but will form a stable transition layer with a gradient density from 0.865 g cm^{-3} to 1.595 g cm^{-3} at room temperature due to the oil miscibility (see Fig. S4A). This enables the buoyant of water droplets (~1.0 g cm^{-3}) at grade, where volume ratio of toluene to CCl_4 is 4:1 and the dynamic viscosity is ~6.66×10^{-4} kg m^{-1} s^{-1}, while immersing in the oil phase. All the spinning FLDs were imaged in the gradient oil using an optical microscope.

Figures and Tables

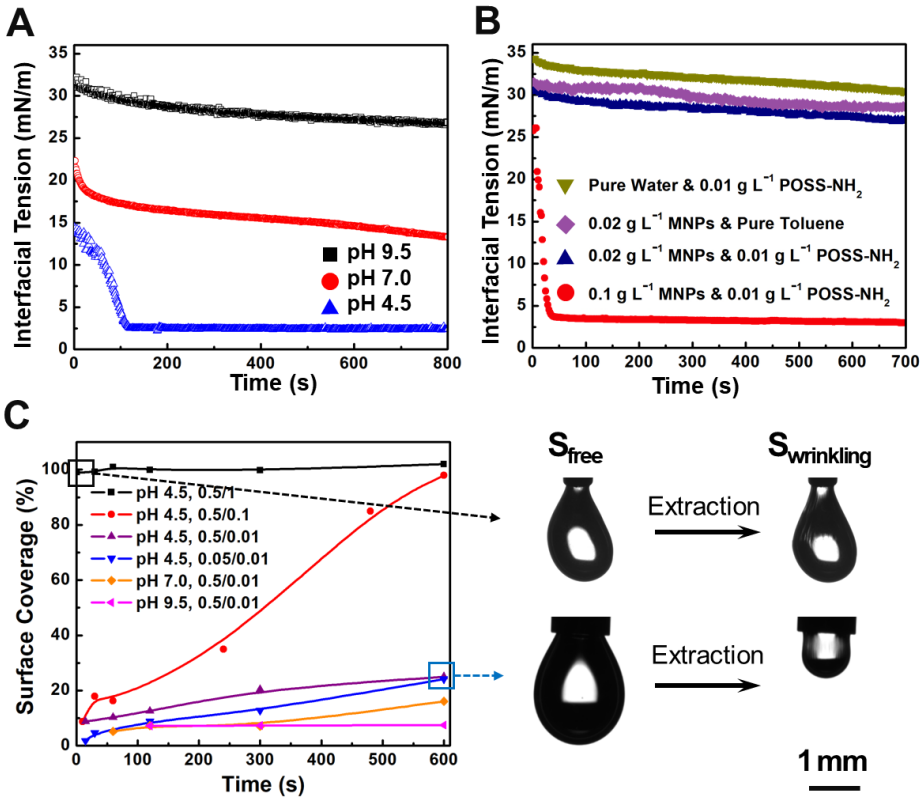

Fig. S1. Temporal evolution of interfacial tension of droplets decorated with MNPs. (A) The influence of pH on interfacial tension is shown for Fe_3O_4-CO_2H MNPs (0.5 g L^{-1}) with POSS-NH_2 (0.01 g L^{-1}). **(B)** Effect of MNPs concentration and respective jamming on interfacial tension for pH 4.5, [POSS-NH_2] = 0.01 g L^{-1}, and [Fe_3O_4-CO_2H MNPs] = 0.02 and 0.1 g L^{-1}. **(C)** Surface coverage of MNPs-surfactants at the water/toluene interface as a function of time for pH 4.5, 7.0, and 9.5, [Fe_3O_4-CO_2H MNPs] = 0.5 or 0.05 g L^{-1}, and [POSS-NH_2] = 0.01, 0.1 or 1 g L^{-1}, respectively. Surface coverage, C_s, is defined as the ratio of surface area at MNPs jamming and free state, respectively, $C_s = S_{wrinkling}/S_{free}$.

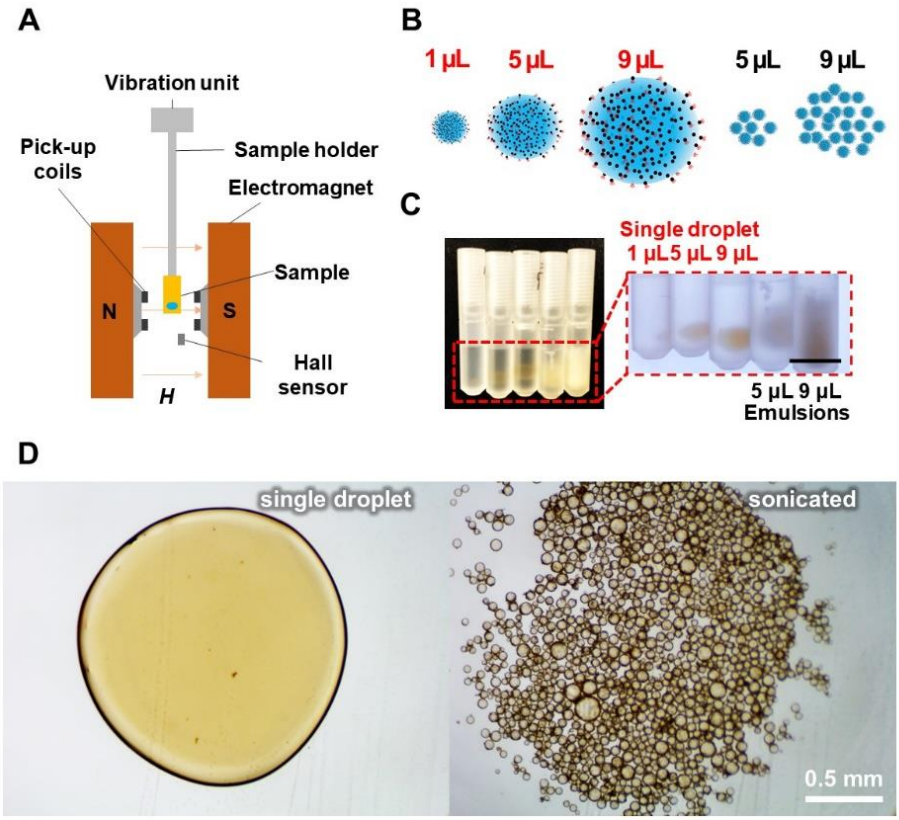

Fig. S2. Vibrating sample magnetometer measurement and liquid sample preparation. (A) Schematics of vibrating sample magnetometer for hysteresis loop measurement. **(B)** Schematics and **(C)** images of single droplets with 1 µL, 5 µL, 9 µL and emulsions of sonicated droplets with 5 µL, 9 µL after being ultrasonicated for 10 s, with the surface to volume ratio, *S*/*V*, increasing ~2 orders in magnitude. Scale bars, 5mm. **(D)** 1-µL droplet with a diameter of ~1.5 mm when spread on a glass microscope slide for observation, the mean size of the droplet is ~50 µm after sonication. Scale bar: 0.5 mm.

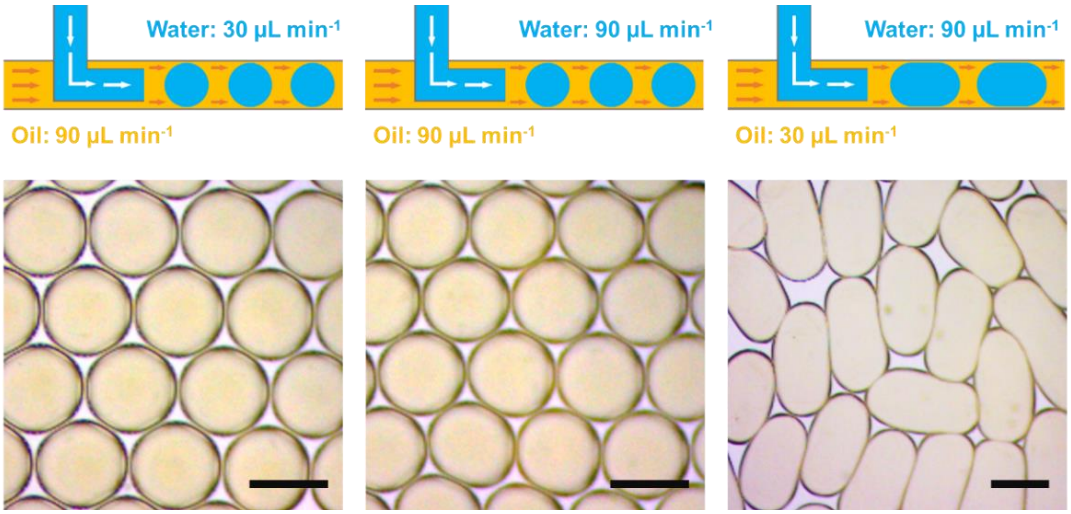

Fig. S3. Shaping droplets by all-liquid 3D printing in microfluidic devices. Shape of the droplets can be optimized by changing diameter and length of PTFE tube, where oil and water mix and flow, and pump-controlled flow rate of water and oil phases. [Fe_3O_4-CO_2H MNPs in water] = 0.5 g L^{-1}, pH 4.5; [POSS-NH_2 in toluene] = 10 g L^{-1}. The printed droplets can be collected using petri dish. Scale bars: 1 mm.

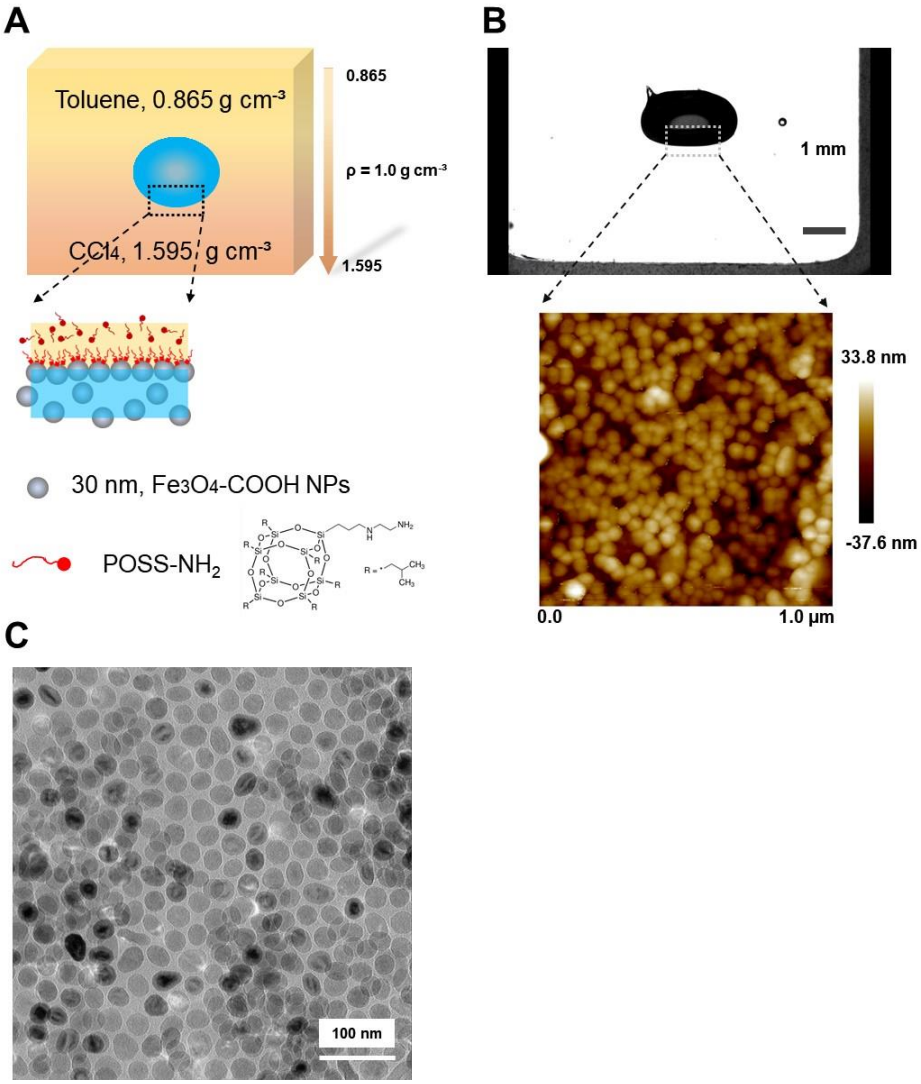

Fig. S4. A droplet buoyant in the gradient oil and morphology of MNPs at interfaces. (A) carboxylated iron oxide nanoparticles (Fe_3O_4-CO_2H MNPs) assemble with amine functionalized POSS (POSS-NH_2) at the water/toluene interface. The aqueous droplet (1.0 g cm^{-3}) is buoyant in the bilayer oil mixture of toluene and CCl_4 (v/v=4:1) with a density gradient without any fierce shaking. **(B)** Side-view backlight image of buoyant droplet, stable in the non-spherical shape, indicates that MNPs-surfactants jam at water/oil interfaces very well. The AFM image of the assembled film indicates the jammed state of MNPs at liquid interfaces. The size of nanoparticles is ~30 nm. **(C)** TEM image of jammed MNPs transferred from water-toluene interface to silicon nitride wafer in the dry state.

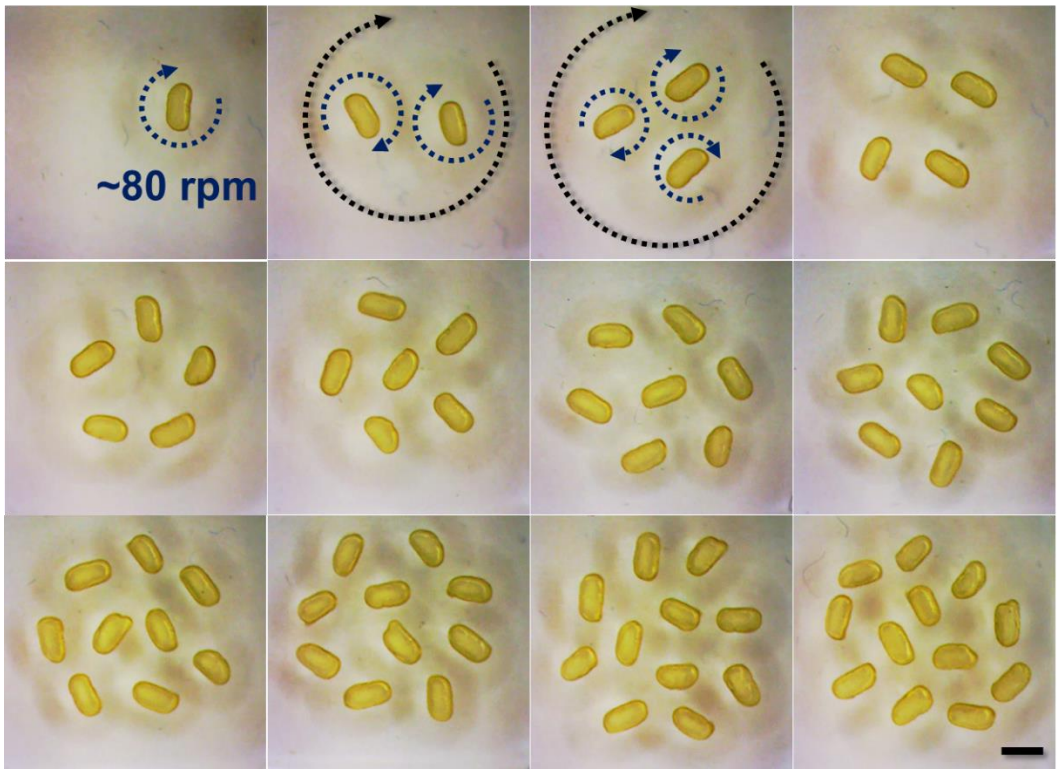

Fig. S5. Top view of stable patterns formed by rotating cylindrical ferromagnetic liquid droplets. Dynamic spinning patterns depend on the droplet numbers (from 1 to 12) and the rotating speed (300 rpm) of the magnet underneath, which generate a rotating magnetic field with a specific strength ($\mu_0 M$ = 1.25 T at surface of the bar magnet). Scale bar: 2 mm.

	Volume (μL)	Saturation Magnetization, M_s ($\times 10^{-8}$ A m^2)	Remanent Magnetization, M_r ($\times 10^{-8}$ A m^2)	Coercivity, H_c (kA m^{-1})	M_r/M_s
Single Droplet	1	1.56	0.48	6.4	0.31
	5	7.86	1.89	7.2	0.24
	9	15.6	4.15	7.2	0.27
Emulsion	5	7.85	1.76	6.0	0.22
	9	14.4	3.70	6.4	0.26

Table S1. Values of saturation magnetization, remanent magnetization, coercive field, and M_r/M_s calculated according to the hysteresis loops.

Movie S1.

A non-magnetized cylindrical ferromagnetic liquid droplet buoyant in the oil is attracted into the solenoid once magnetic field is applied. We observe that the printed FLD cylinder enter into the solenoid with an acceleration after a current is applied to the solenoid to generate a gradient magnetic field. Magnetization happens at first then the attraction makes effect. The video is played with 4 times speed up. The length of the FLD cylinder is 2 mm.

Movie S2.

A magnetized cylindrical ferromagnetic liquid droplet buoyant in the oil is attracted into the solenoid faster. The magnetized FLD cylinder interacts with solenoid by north-south attraction initially, and reaches to the solenoid faster without the magnetization process. The video is played with 4 times speed up. The length of the FLD cylinder is 2 mm.

Movie S3.

A magnetized cylindrical ferromagnetic liquid droplet buoyant in the oil is attracted into the solenoid slower. The repositioned magnetized FLD cylinder rotates to align with the field flux at first due to the south-south repulsion, and then reaches to the solenoid under the north-south attraction. The dipole moment of the FLD cylinder is fixed very well by the interfacial jammed magnetic nanoparticle surfactants. The video is played with 4 times speed up. The length of the FLD cylinder is 2 mm.

Movie S4.

Magnetic N-S dipole interactions between two FLDs. Two magnetized liquid cylinders buoyant in the oil attract each other by coordinated actions of north-south dipole attraction and north-north, south-south repulsions. The video is played at 6 times the actual speed. The volume of the FLD droplets is 2μL and the length of the FLD cylinder is 2 mm.

Movie S5.

Deformation of spherical ferromagnetic liquid droplet into cylindrical shape. A spherical ferromagnetic liquid droplet was drawn into the glass capillary and deformed into a cylindrical shape. The reshaped ferromagnetic liquid droplet was able to rotate, following with the external spinning magnetic field. The video is played at 3 times actual speed. The volume of the ferromagnetic liquid droplet is 2μL and the length of the ferromagnetic liquid cylinder is 2 mm.

Movie S6.

Ferromagnetic liquid droplets are separated from the other paramagnetic liquid droplets by static permanent magnet. The brown spherical FLD droplets with MNPSs jammed at water/oil interfaces move faster after being magnetized than the FF droplets. Separation from the other magnetic droplets is well controlled by external static and rotating magnetic field. The video is played with 2 times speed up. The diameter of droplets is 1 mm.

Movie S7.

A drop of Nile Red toluene solution is added into the gradient oil phase to visualize the flow fields around vortex-generating FLDs. We observe the hydrodynamic radius of a spinning FLD cylinder clearly. The clockwise fluid flow around every FLD s generated vortex-vortex repulsion,

leading to the dynamic pattern formation in couple with the magnetic attractions from the rotating magnet. The video is in real time. Scale bar, 2 mm.

Movie S8.

A dynamic pattern is formed by 12 rotating FLD cylinders buoyant in the surrounding oil phase. These patterns are similar with those of Mayer's floating magnets. The attraction to the center of bar magnet and the repulsions between each FLD s result in the special pattern where each FLD stays in the same position relatively. The video is in real time. The length of the FLD cylinder is 2 mm

Movie S9.

Manipulating the orientation of FLD cylinders with an external magnetic field generated by a bar magnet. All magnetized liquid cylinders are aligned along the direction of flow field. They can re-orient immediately along with the changing direction of external magnetic field. The video is in real time. The length of the ferromagnetic liquid cylinder is 2 mm.

Movie S10.

Ferromagnetic liquid droplets are separated from the other paramagnetic liquid droplets by rotating permanent magnet. The spherical FLD droplets with dipole moment rotate along with the rotating magnetic field and form patterns due to the hydrodynamic repulsion and magnetic attraction. The red and fluorescent green paramagnetic droplets without dipole moment only move along with the rotating field randomly, and are expelled from the central area by the vortex flow. The video is played with 6 times speed up. The diameter of droplets is 1 mm.

References and Notes

1. S. Odenbach, Ferrofluids and their applications. *MRS Bull.* **38**, 921–924 (2013).

2. R. E. Rosensweig, "Magnetic fluids" in *Ferrohydrodynamics* (Courier Corporation, 2013), pp. 34–44.

3. M. Cui, T. Emrick, T. P. Russell, Stabilizing liquid drops in nonequilibrium shapes by the interfacial jamming of nanoparticles. *Science* **342**, 460–463 (2013).

4. Z. Zhang, Y. Jiang, C. Huang, Y. Chai, E. Goldfine, F. Liu, W. Feng, J. Forth, T. E. Williams, P. D. Ashby, T. P. Russell, B. A. Helms, Guiding kinetic trajectories between jammed and unjammed states in 2D colloidal nanocrystal-polymer assemblies with zwitterionic ligands. *Sci. Adv.* **4**, p8045 (2018).

5. A. H. Lu, E. L. Salabas, F. Schüth, Magnetic nanoparticles: Synthesis, protection, functionalization, and application. *Angew. Chem. Int. Ed.* **46**, 1222–1244 (2007).

6. J. J. Benkoski, S. E. Bowles, B. D. Korth, R. L. Jones, J. F. Douglas, A. Karim, J. Pyun, Field induced formation of mesoscopic polymer chains from functional ferromagnetic colloids. *J. Am. Chem. Soc.* **129**, 6291–6297 (2007).

7. R. Streubel, N. Kent, S. Dhuey, A. Scholl, S. Kevan, P. Fischer, Spatial and temporal correlations of XY macro spins. *Nano Lett.* **18**, 7428–7434 (2018).

8. E. C. Stoner, E. P. Wohlfarth, A mechanism of magnetic hysteresis in heterogeneous alloys. *Philos. Trans. R. Soc. Lond. A* **240**, 599–642 (1948).

9. W. Luo, S. R. Nagel, T. F. Rosenbaum, R. E. Rosensweig, Dipole interactions with random anisotropy in a frozen ferrofluid. *Phys. Rev. Lett.* **67**, 2721–2724 (1991).

10. G. F. Goya, T. S. Berquó, F. C. Fonseca, M. P. Morales, Static and dynamic magnetic properties of spherical magnetite nanoparticles. *J. Appl. Phys.* **94**, 3520–3528 (2003).

11. X. Liu, S. Shi, Y. Li, J. Forth, D. Wang, T. P. Russell, Liquid tubule formation and stabilization using cellulose nanocrystal surfactants. *Angew. Chem. Int. Ed.* **56**, 12594–12598 (2017).

12. J. Forth, X. Liu, J. Hasnain, A. Toor, K. Miszta, S. Shi, P. L. Geissler, T. Emrick, B. A. Helms, T. P. Russell, Reconfigurable printed liquids. *Adv. Mater.* **30**, e1707603 (2018).

13. S. Shi, X. Liu, Y. Li, X. Wu, D. Wang, J. Forth, T. P. Russell, Liquid Letters. *Adv. Mater.* **30**, 1705800 (2018).

14. A. Toor, S. Lamb, B. A. Helms, T. P. Russell, Reconfigurable microfluidic droplets stabilized by nanoparticle surfactants. *ACS Nano* **12**, 2365–2372 (2018).

15. L. Derr, A photographic study of mayer's floating magnets. *Proc. Am. Acad. Arts Sci.* **44**, 525–528 (1909).

16. B. A. Grzybowski, H. A. Stone, G. M. Whitesides, Dynamic self-assembly of magnetized, millimetre-sized objects rotating at a liquid-air interface. *Nature* **405**, 1033–1036 (2000).

17. W. Wang, J. Giltinan, S. Zakharchenko, M. Sitti, Dynamic and programmable self-assembly of micro-rafts at the air-water interface. *Sci. Adv.* **3**, e1602522 (2017).

18. J. V. I. Timonen, M. Latikka, L. Leibler, R. H. A. Ras, O. Ikkala, Switchable static and dynamic self-assembly of magnetic droplets on superhydrophobic surfaces. *Science* **341**, 253–257 (2013).

19. N. C. Keim, P. E. Arratia, Mechanical and microscopic properties of the reversible plastic regime in a 2D jammed material. *Phys. Rev. Lett.* **112**, 028302 (2014).

20. H. Xu, S. Melle, K. Golemanov, G. Fuller, Shape and buckling transitions in solid-stabilized drops. *Langmuir* **21**, 10016–10020 (2005).